AIAA JOURNAL
Vol. 42, No. 9, September 2004

Buffeting Flows over a Low-Sweep Delta Wing

G. S. Taylor* and I. Gursul†
University of Bath, Bath, England BA2 7AY, United Kingdom

An experimental study was conducted with the aim of understanding the unsteady vortex flows and buffeting response of a nonslender delta wing with 50-deg leading-edge sweep angle. Particle image velocimetry and laser Doppler velocimetry measurements, surface flow visualization, force balance measurements, and wing-tip acceleration measurements were used. It was found that there is a profound effect of Reynolds number on the structure of vortical flows. The breakdown of the leading-edge vortices is delayed significantly, and the vortices form more inboard at low Reynolds numbers. The secondary vortex effectively splits the primary vortex into two separate concentrations of vorticity, resulting in a dual vortex structure at small incidences. This dual vortex structure diminishes, and a single primary vortex is observed at higher incidences. At higher Reynolds numbers (on the order of 3×10^4) the flow approaches an asymptotic state, with further increases in the Reynolds number resulting in only small variations in the location of vortex core and breakdown. Weak vortex breakdown observed at low incidences is replaced by a conical breakdown with increasing incidences. However, the maximum buffeting occurs prior to the stall, after the vortex breakdown has reached the apex of the wing. The largest velocity fluctuations near the wing surface are observed along the reattachment line. Hence, the shear-layer reattachment, rather than the vortex breakdown phenomenon, is the most important source of increasing buffet in the prestall region as incidence is increased. The velocity fluctuations in the reattachment region have similar dominant frequencies as slender wings in spite of the differences in the physical nature of the flow. With further increase in incidence, the shear-layer reattachment becomes impossible, resulting in very low velocity fluctuations near the wing surface and a precipitous fall in the rms wing-tip acceleration.

Nomenclature

C_L	=	lift coefficient
C_{LMAX}	=	maximum lift coefficient
C_{Mapex}	=	nose-up pitching-moment coefficient taken about apex
c	=	chord length
f	=	frequency
q	=	freestream dynamic pressure ($\rho_\infty U_\infty^2/2$)
Re_c	=	Reynolds number based on chord length
S	=	wing reference area
s	=	semispan
t	=	wing thickness
U_∞	=	freestream velocity
u	=	velocity
x	=	axial coordinate
y	=	spanwise coordinate
α	=	angle of attack
Λ	=	leading-edge sweep angle
ρ_∞	=	density of freestream
ϕ	=	angle between particle-image-velocimetry measurement plane and freestream

Introduction

THE vortical flow over nonslender delta wings ($\Lambda \leq 55$ deg) has recently become a topic of increased interest in literature. Projected uses for such low-sweep planforms include unmanned air vehicle and micro air vehicle designs. Although the flow topology over more slender wings, typically $\Lambda \geq 65$ deg, has been extensively studied and is now reasonably well understood,[1–3] the flow over lower sweep wings has attracted less attention in the literature until recently.

Received 30 September 2003; revision received 6 April 2004; accepted for publication 29 April 2004.

*Postdoctoral Research Associate, Department of Mechanical Engineering. Member AIAA.

†Professor of Aerospace Engineering, Department of Mechanical Engineering. Associate Fellow AIAA.

Early work in the field[4] reported that the vortex core was very unsteady and the vortex breakdown was difficult to identify for sweep angles of 55 and 45 deg. Wentz and Kohlman[5] indicated that the vortex breakdown was only observed in a region close to the apex for $\Lambda = 50$ deg wing. Both studies, which were conducted at Reynolds numbers on the order of 10^6, concluded that the location of breakdown could not be found for $\Lambda = 45$ deg wing, indicating that it was very close to the apex of the wing.

Although leading-edge vortices seem to be breaking early at high Reynolds numbers, well-defined vortices were visible at low Reynolds numbers ($Re = 7 \times 10^3$ in Ref. 6 and $Re = 8.5 \times 10^3$ in Ref. 7) for $\Lambda = 50$ deg. At these very low Reynolds numbers, vortices can have wake-like axial velocity profiles even upstream of breakdown.[7] The vortices form much closer to the surface of the wing,[8] and vortex/boundary-layer interaction becomes important at low Reynolds numbers.[9,10]

However, evidence suggests that at high Reynolds numbers vortex breakdown occurs close to the apex of the wing even at small incidences such as a few degrees. Although substantial differences from the breakdown of slender vortices are predicted,[10] the results suggest highly unsteady flows over the wing. With increasing angle of attack, vortex breakdown reaches the apex, and the separated shear layers become the dominant feature of the flow. Very little is known about the structure and characteristics of unsteady flow phenomena over nonslender delta wings. Much existing knowledge on vortex flows is related to slender vortices. A number of unsteady phenomena are known to exist over slender delta wings, such as vortex wondering,[11] helical mode instability,[12,13] shear-layer instabilities,[14] vortex interactions,[15] and at high incidences vortex shedding.[16] The role of these instabilities in buffeting of slender wings is well understood. The most important source of buffeting is the vortex breakdown and the helical mode instability. Even for a $\Lambda = 60$-deg wing, which can be regarded as the transitional case between the slender wing and nonslender wings, it was found that maximum rms buffeting[17] occurs when vortex breakdown is close to the apex of the wing. The rms acceleration drops very rapidly in the vortex shedding regime at higher angles of attack.

However, for nonslender delta wings it is not known whether vortex breakdown is the main source of buffeting, given that there are substantial differences in the structure of vortices and breakdown. More importantly, vortex breakdown reaches the apex of the wing at

relatively small angles of attack. Whether any of the instabilities just cited for slender wings, either alone or in combination, play any role in buffeting of nonslender wings remains unknown. For example, it was surprising that evidence of unsteady vortex interactions[17] (between the left and right sides of the wing) was found for a relatively low sweep angle of $\Lambda = 60$ deg, as this kind of interaction was believed to be limited to slender wings.[15] Also, for nonslender wings with relatively large spans, a coupling between the wing structure[18] and unsteady flow phenomena can be important.

The aim of this paper is to present the results of an experimental study into the characteristics of unsteady vortex flows and buffeting of a wing with 50-deg leading-edge sweep. Particle image velocimetry (PIV) and laser Doppler velocimetry (LDV) measurements, surface flow visualization, force balance measurements, and wing-tip acceleration measurements were combined in order to both document the unsteady flows and understand the buffeting response.

Experimental Setup

Both wind-tunnel and water-tunnel experiments were conducted. Water-tunnel experiments were performed in the facility at the University of Bath. The tunnel is an Eidetics Model 1520 free-surface tunnel with a 0.381×0.508 m working section and can achieve speeds up to 0.45 m/s through a closed-circuit continuous flow system. The tunnel has four viewing windows; three surrounding the test section and one downstream allowing axial viewing. The height of the test section above the floor allows flow visualization from below as well as from the sides. A schematic of the water-tunnel setup is shown in Fig. 1a. In water-tunnel experiments, the freestream velocity was varied in the range $U_\infty = 0.05 - 0.4$ m/s, giving Reynolds numbers in the range $Re_c = 4.3 \times 10^3 - 34.7 \times 10^3$. The majority of the velocity measurements were carried out for $Re_c \approx 2.6 \times 10^4$. The maximum blockage ratio was around 1.5% at $\alpha = 25$ deg. The water-tunnel model, used in PIV and LDV experiments, is shown in Fig. 1b. Each edge of the model had a 45-deg bevel on the pressure surface, including the trailing edge. The model was mounted in the tunnel using a sting projecting from the rear of the model, as shown in Fig. 1b. The sting was attached to the model using screws countersunk into the models suction surface. The model had a chord length $c = 89$ mm and a thickness $t = 2$ mm, giving a thickness to chord ratio $t/c = 2.2\%$.

Visualization of the vortex trajectories was achieved using food coloring diluted 1:4 with water. The dye was injected into the flow near the apex of the models via a pressurized delivery system incorporating simple gate valves to control the exit velocity of the fluid. To ensure that the dye itself did not affect the formation of the vortices over the leading edges, the exit velocity was carefully controlled. Thin metal tubes were used to transport the dye to the apex of the models. A digital video camera with a capture rate of 25 frames per second, and a resolution of 570,000 pixels was used to capture images.

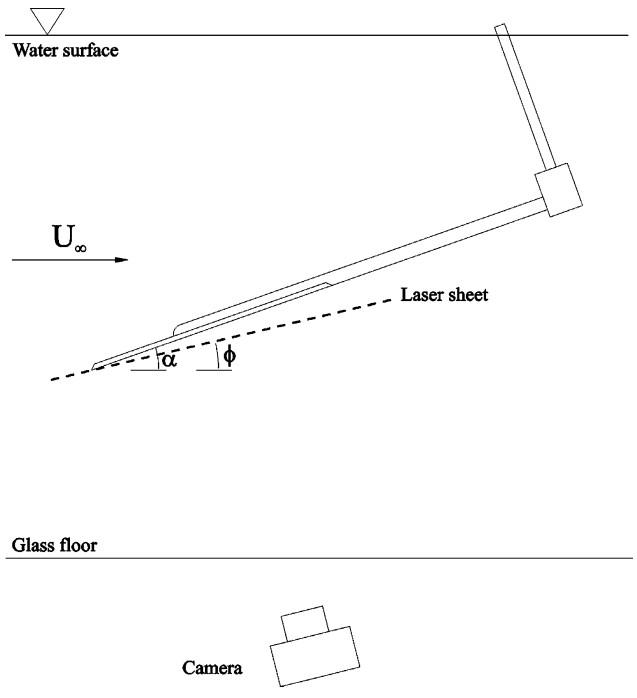

Fig. 1a Schematic of water-tunnel setup and PIV experiments.

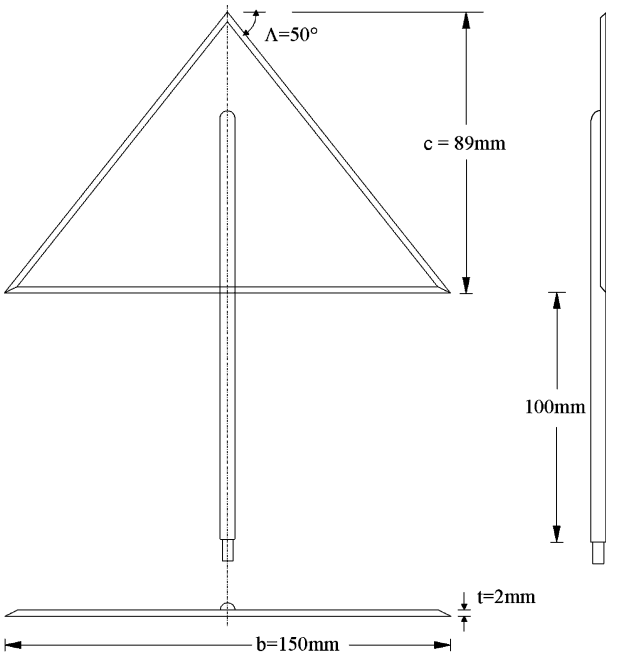

Fig. 1b Main dimensions of the water-tunnel model and support.

Two-dimensional digital-PIV measurements of the flowfield were undertaken in the water tunnel. Illumination of the plane of interest was achieved using a pair of pulsed mini Nd:YAG lasers with a maximum energy of 120 mJ per pulse. A combination of cylindrical and spherical lenses was used to generate a light sheet of sufficient divergence and focus. Images were captured using an eight-bit digital camera with a resolution of 4.2 million pixels. A Hart cross-correlation algorithm[19] was used to analyze the images and to produce velocity vectors suitable for further postprocessing. Each field was averaged over 100 instantaneous frames with an interval between frames of 0.267 s to yield a time average spanning around $90\, c/U_\infty$, and velocity vectors were calculated at over 50,000 points in each field. The flow was seeded with hollow glass particles of mean diameter 4 μm. The velocity field was measured in a plane through the vortex core, which is inclined by an angle ϕ with respect to the freestream velocity as shown in Fig. 1a. Also, velocity was measured in a plane parallel to the wing surface at a 1 mm distance to reveal the near-surface flow pattern. All PIV data were taken at a freestream velocity of $U_\infty = 0.3$ m/s, corresponding to $Re_c = 2.67 \times 10^4$.

The spectral content of the velocity in these two planes was investigated by using a two-component LDV system, which consisted of a 300-mW, air-cooled argon-ion laser and TSI burst correlator unit. The data rate was of the order of 400 Hz with a burst efficiency of approximately 50%, and a total of 20,000 data points was recorded for each test giving a sample period of well over $100\, c/U_\infty$.

Wind-tunnel experiments were conducted in the high-speed working section of the 2.13×1.52 m closed-circuit facility. Models were supported using the high-incidence rig as shown in Fig. 2a. Experiments were conducted at a constant freestream velocity of $U_\infty = 30$ m/s, giving Reynolds numbers $Re = 6.6 \times 10^5$ and one million for two models tested. Maximum blockage for the wind tunnel was approximately 3.4% at $\alpha = 35$ deg. In the wind tunnel a flexible wing (see Fig. 2b) made of aluminum was used for measurements of the buffeting response, and a rigid wing was used for

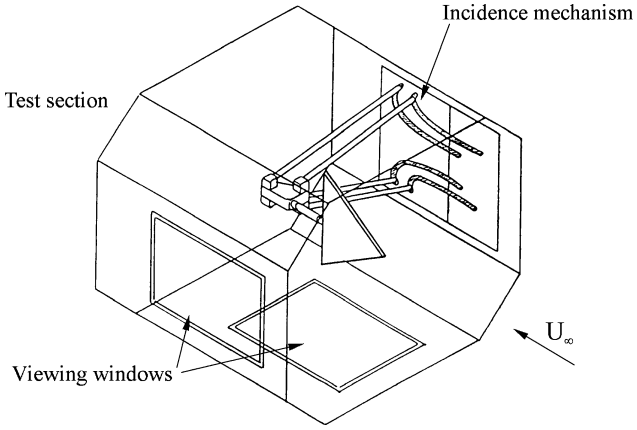

Fig. 2a Schematic of wind-tunnel setup and rigid wing.

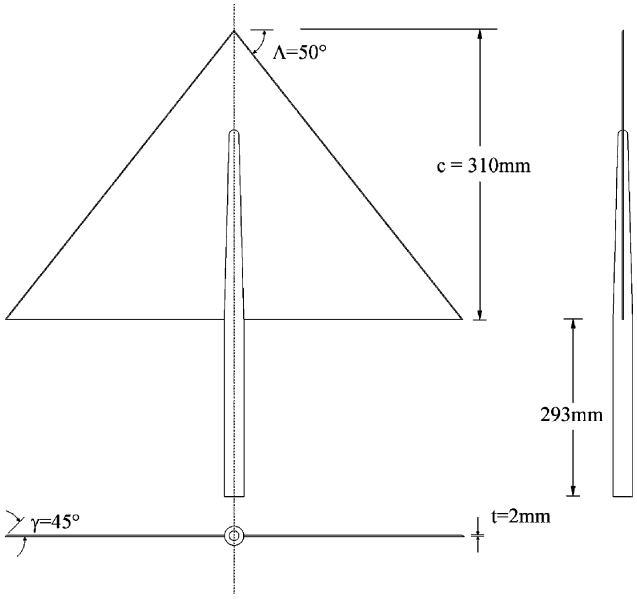

Fig. 2b Main dimensions of flexible wing and support.

surface flow visualization. The model used for measuring buffeting response is slightly flexible, with the maximum tip deflection less than 1% of the chord length. The rigid wing had a chord length of $c = 475$ mm and a thickness-to-chord ratio of $t/c = 3.6\%$, while the flexible wing had a chord length of $c = 310$ mm and a thickness-to-chord ratio of $t/c = 0.65\%$. All models had a 45-deg bevel on leading edges.

Surface flow visualizations were performed in the wind tunnel using a fine fluorescent powder paint mixed 2:1 with paraffin. The paint was applied over the wing surface using an air spray gun. Images of the resulting visualizations were captured using the digital video camera, which was interfaced to a desktop computer via a commercially available digital video capture board.

Buffeting response was measured by mounting Entran EGA miniature accelerometers with a mass of approximately 0.5 g on the tips of the flexible wing. Force balance measurements were undertaken using a six-component, strain-gauged internal balance. Signals from the accelerometers and force balance were recorded using a desktop PC with a 12-bit A/D data-acquisition card. Signals were recorded for a period of 20 s at a sampling frequency of 1000 Hz, resulting in a record spanning over 1000 c/U_∞. Nose-up pitching moments are calculated about the apex and are normalized by qSc.

Results

Overview of Vortical Flows

In initial experiments, dye flow visualization was used to study the behavior of the leading-edge vortices for a range of incidences and Reynolds numbers.[9] Here a summary of these findings will be presented. The images in Fig. 3 show the vortices generated over the wing at an incidence of $\alpha = 5$ deg for three different Reynolds numbers. Vortex breakdown of leading-edge vortices at the trailing edge of the wing is visible for $Re_c = 8.7 \times 10^3$. A further increase in Reynolds number resulted in the upstream progression of the breakdown of the vortices, which is a curious result considering the accepted insensitivity of vortices and vortex breakdown over more slender wings. When the Reynolds number is nearly tripled to $Re_c = 2.6 \times 10^4$, the vortex breakdown location moves to nearly 40% of the chord length. At low Reynolds numbers the breakdown, when present, appeared to be more axisymmetric in nature, and the

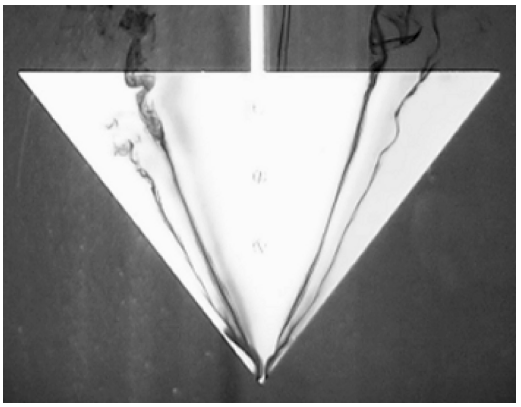

$Re = 8.7 \times 10^3$

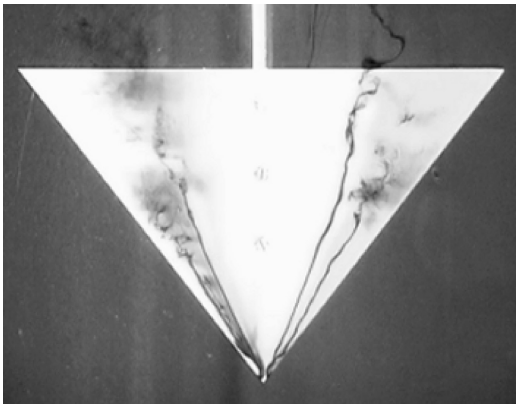

$Re = 1.3 \times 10^4$

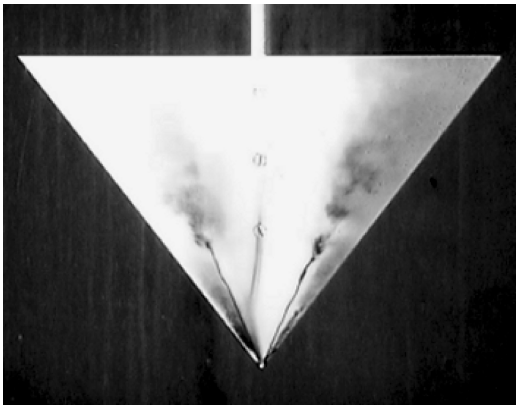

$Re = 2.6 \times 10^4$

Fig. 3 Dye flow visualization of vortex flows for $\alpha = 5$ deg in water-tunnel experiments.

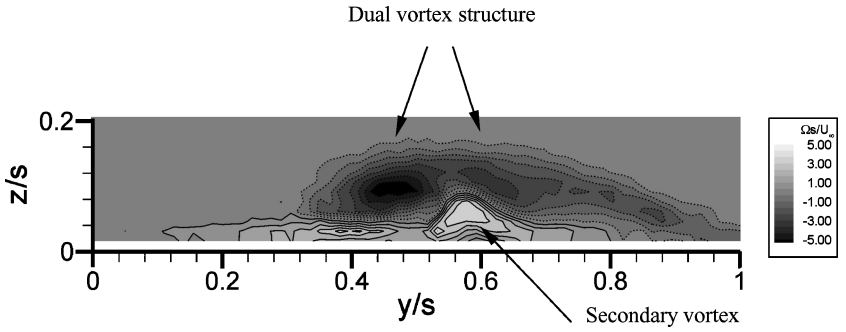

Fig. 4 Crossflow vorticity field at $x/c = 0.4$, $\alpha = 7.5$ deg, $Re_c = 8.7 \times 10^3$, showing dual vortex structure.

transition from coherent to broken vortex was rapid. However, at the higher Reynolds numbers, the form of the breakdown became less clear, and the transition seemed to be less abrupt.

Also apparent under these conditions was the formation of an additional vortex outboard of the primary vortex, which indicated the existence of a dual vortex structure (a pair of corotating vortices) that has also been observed in a previous computational study.[10] The images presented in Fig. 3 indicate that the outboard pair of vortices undergoes breakdown further upstream than the primary (inboard) pair in all of the cases considered herein. At relatively small incidences and low Reynolds numbers, this dual vortex structure was typical. As an example, Fig. 4 shows contours of constant axial vorticity in the cross-flow plane at $x/c = 0.4$ for $\alpha = 7.5$ deg and $Re_c = 8.7 \times 10^3$. The primary vortex is clearly shown as the large concentration of vorticity centred at about $y/s = 0.5$. The secondary separation is identified as a region of vorticity, of opposite sign, just outboard of the primary vortex. However, this figure also demonstrates clearly the dual vortex structure, with a third concentration of vorticity, with a sign consistent with the primary vortex but significantly weaker, just outboard of the secondary vortex. Outboard of this lies a region of distributed vorticity associated with the separated shear layer. Hence, the first experimental evidence of the dual vortex structure with the same sign of vorticity upstream of breakdown is presented in this study. Multiple corotating vortices were observed on the 60-deg sweep wing of the F-106B airplane.[20] It was concluded in this reference that these multiple vortices are likely attributed to small surface distortions in the wing leading-edge region and hence appear to be caused by a different mechanism.

The vortical flow structure is strongly affected by Reynolds number. A single layer of vorticity concentration was observed at very low Reynolds numbers (on the order of few thousands), and the dual vortex structure was absent. With increasing Reynolds number, the significant interaction between the boundary layer and primary vortex results in this dual vortex structure. With further increases in Reynolds number, the weaker vortex tends to break down significantly earlier than the primary vortex as shown in Fig. 3.

Another important parameter that affects the structure of vortical flow is angle of attack, as shown in Fig. 5 for $Re_c = 1.3 \times 10^4$. It is seen that the breakdown of the leading-edge vortices progressed forward as the incidence of the wing was increased. As observed previously, in all of these cases the weaker vortex breaks down upstream of the primary vortex. With increasing incidence, the vortical layer is located farther away from the wing and boundary layer, and hence the dual vortex structure is less likely to develop; this is evidenced by the seemingly weaker formation of the outboard vortices at higher incidences. Another interesting feature was the occurrence of breakdown over the wing at $\alpha = 2.5$ deg. At such a low incidence one would not normally expect to observe breakdown, especially so far forward on the wing. Compared to vortices over slender wings, early breakdown of vortices at low incidences can be because of the stronger adverse pressure gradient because of the trailing edge. In all cases, large fluctuations in the breakdown location of the primary vortex were observed.[9] The rms breakdown location was calculated for both primary leading-edge vortices at $Re_c = 2.67 \times 10^4$ from the time history of breakdown locations and was found to be

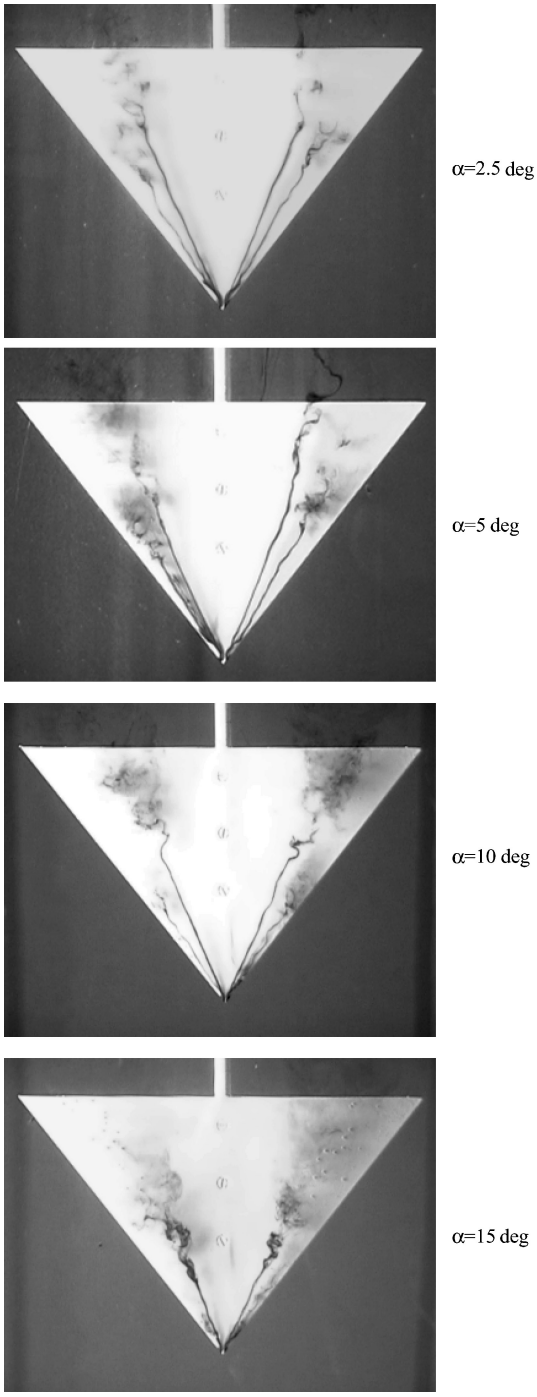

Fig. 5 Water-tunnel flow visualization pictures of vortex breakdown for varying incidence, $Re = 1.3 \times 10^4$.

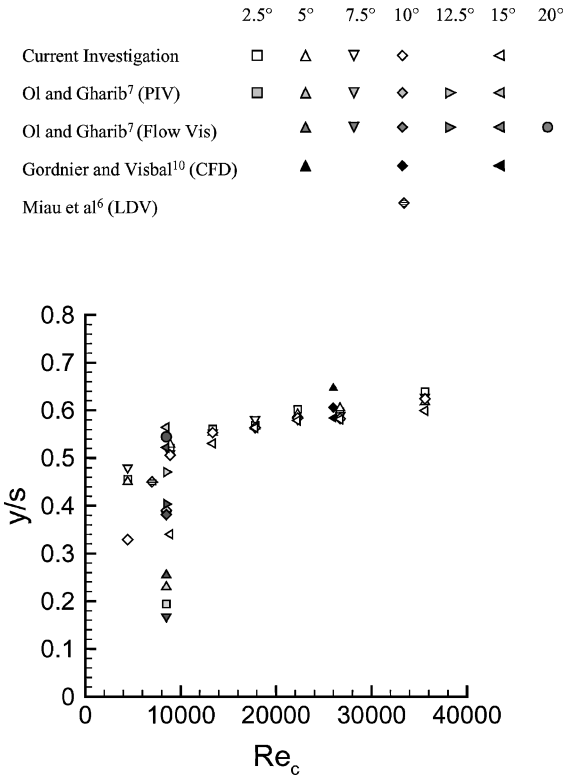

Fig. 6 Variation of spanwise location of vortex core with Reynolds number; sweep angle of 50 deg.

independent of incidence, being roughly equal to $(x_{BD}/c)_{rms} \approx 0.06$. This is significantly greater than $(x_{BD}/c)_{rms} \approx 0.03$ observed over more slender planforms.[15]

Further effects of Reynolds number have also been identified. It was observed that the spanwise location of the vortex core moved outboard as the Reynolds number increased. A similar effect was also observed over more slender wings.[21] This variation in the location of the vortex core is plotted for all incidences in Fig. 6 and compared with data presented in the literature.[6,7,10] Ol and Gharib[7] state that the qualitative features of the flow, such as the location of the primary vortex, do not change significantly with Reynolds number, even as low as $Re_c = 6.2 \times 10^3$. In the present experiments, however, a clear shift of vortex location was observed as the Reynolds number was varied. At higher Reynolds numbers (on the order of 3×10^4) the flow approaches an asymptotic state, with further increases in the Reynolds number resulting in only small variations in the location of vortex core and breakdown. A strong dependence of the vortex trajectory on incidence was also noted at low Reynolds numbers, and a degree of scatter exists in the data indicating that the flow might be sensitive to small changes in experimental setup and measurement technique. As Reynolds number was increased, this sensitivity of the vortex trajectory to incidence reduced, which is consistent with the inviscid theory of Moore and Pullin.[22] The computational results of Gordnier and Visbal[10] compare well with the experimental results of this investigation, although they exhibit slightly larger variation with incidence at the Reynolds number considered.

Buffeting Response

Figure 7 shows the variation of the rms acceleration of the wing tip with angle of attack. Buffeting at low incidences is small and is similar to the level observed for a $\Lambda = 60$ deg wing[17] with the same thickness and span. With increasing angle of attack, there is an increase in the slope of the buffeting response curve at around $\alpha \approx 7$ deg, followed by a significant increase in the buffeting response. The rms acceleration reaches a maximum of around 70 m/s^2 at around $\alpha = 19$ deg. This maximum value is slightly lower than that of the $\Lambda = 60$ deg wing, indicating that buffeting response decreases slightly with decreasing sweep angle. A further increase in incidence beyond $\alpha \approx 21$ deg results in a sudden reduction in the vibration of the wing tip, and by $\alpha = 23$ deg the level has dropped to around a third of its peak value. This sudden drop, which signals the transition to the vortex-shedding regime, is qualitatively similar to that of the $\Lambda = 60$ deg wing.

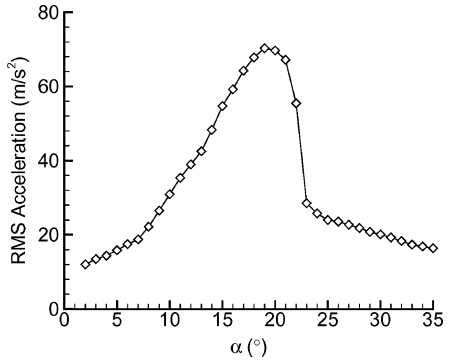

Fig. 7 Variation of wing-tip rms acceleration with incidence for flexible model in wind-tunnel experiments, $Re = 6.6 \times 10^5$.

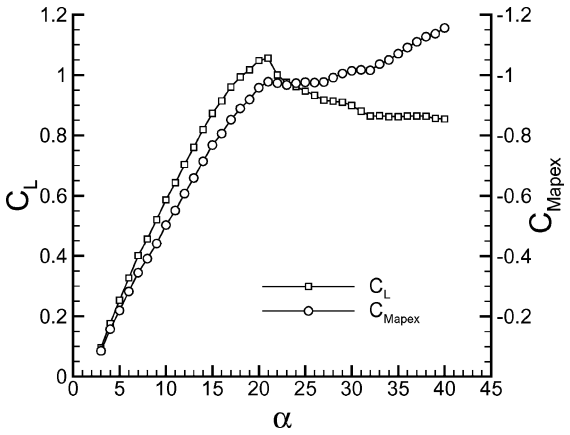

Fig. 8 Variation of C_L, C_{Mapex} with incidence for flexible model in wind-tunnel experiments, $Re = 6.6 \times 10^5$.

To reveal the relationship between the buffeting response and time-averaged aerodynamic forces, the variation of lift coefficient C_L and pitching-moment coefficient about the apex C_{Mapex} with incidence is shown in Fig. 8 for the flexible wing. The data reveal that the wing encounters stall at around $\alpha = 21$ deg, which is slightly lower than expected from the results of Earnshaw and Lawford,[4] who found a similar stall angle for a rigid wing of 45-deg leading-edge sweep. The maximum lift generated by the wing is $C_{LMAX} = 1.07$, which is roughly as expected.[4] The reduction in lift associated with the stall is accompanied by a flattening of the nose-up pitching moment, but no significant reduction was observed. Comparison of Figs. 7 and 8 reveals the correlation between the stall angle and the drop in tip vibration. Maximum excitation of the tip occurs in the flattened region of the lift curve, prior to the stall. Between the point of maximum buffeting and the point at which the wing completely stalls lies the large reduction in rms tip acceleration. It is therefore evident that it is some characteristic of the prestall flow that is responsible for the excitation of the wing tip.

Time-Averaged Flow

Further investigation of the vortical flow was undertaken with the PIV measurements in the water tunnel. Figure 9 shows the magnitude of the time-averaged velocity in a plane through the vortex core (this plane is illustrated in Fig. 1a for clarity). For $\alpha = 10$ deg, there is no indication of vortex breakdown, although flow visualization revealed the bubble-like breakdown at a time-averaged location of $x/c \approx 0.40$. Hence both upstream and downstream of breakdown

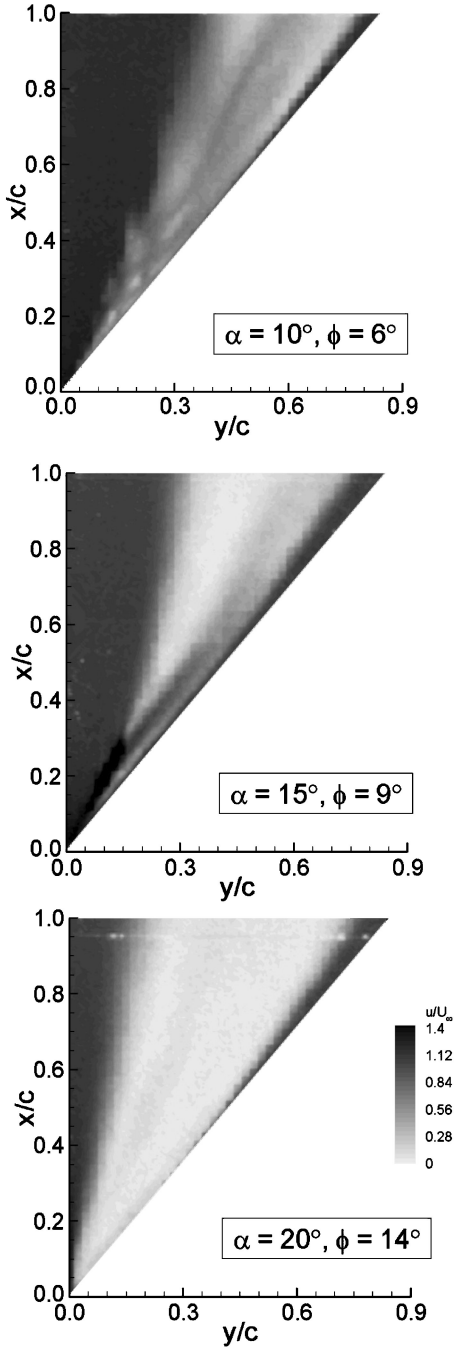

Fig. 9 Magnitude of velocity in a plane through the vortex core in water-tunnel experiments.

there exists wake-like axial flow. The swirl angle or ratio (maximum value of the ratio of swirl velocity to axial velicity) might be large because of the wake-like axial velocity, which might also contribute to vortex breakdown at low incidences. Very low-velocity regions are visible for $x/c \geq 0.7$, but there is again no evidence of a breakdown based on velocity magnitude shown in Fig. 9. In general, at small incidences vortex breakdown is weak and difficult to identify, as there is no complete flow stagnation. At $\alpha = 15$ deg, a clearly defined jet-like axial flow in the vortex core and a clear breakdown region are observed. Hence, there are some similarities to slender wings at relatively higher incidences, but the breakdown is not as abrupt as those observed over slender delta wings. The breakdown region is conical in shape, with an apparent inboard shift of the vortex axis after breakdown. These features were also observed in recent computational simulations.[10] At $\alpha = 20$ deg, the vortex structure has broken down, and a large conical region of stagnant flow is observed. The largest buffeting of the flexible wing occurs around this angle of attack.

Surface Flow Pattern

An indication of the near-surface flow pattern was obtained from the PIV measurements in a plane parallel to the wing surface. Magnitudes of the time-averaged velocity and streamline pattern are shown in Fig. 10 for $\alpha = 10$, 15, 20, and 25 deg. For $\alpha = 10$ deg, the "footprint" of the vortex was bounded by the shear-layer reattachment line to the inboard side and by the secondary separation line on the outboard side. The attachment and separation lines are identified by the divergence or convergence of streamlines in the surface flow. (A fuller description of the interpretation of surface topology can be found in Ref. 23.) Flow inboard of the primary reattachment line was largely unaffected in terms of direction, albeit of reduced velocity compared with the freestream. A region of reduced velocity was observed coincident with the secondary separation line. The primary reattachment and secondary separation lines are most distinct at $\alpha = 15$ deg. Increasing incidence moved the primary reattachment line inboard toward the wing centerline. The stagnant region increases in size as incidence is increased. Note that the largest buffeting of the flexible wing occurs around $\alpha = 20$ deg. At the largest incidence $\alpha = 25$ deg, the shear-layer reattachment fails entirely, being replaced by a flow feature described in previous research[4] as a "whorl."

Surface flow visualization was also performed for the rigid wing in the wind tunnel. The results of these experiments are shown in Fig. 11. The surface flow patterns clearly show the existence of the primary reattachment and secondary separation lines even at low incidences, indicating the presence of strong vortical flows over the lifting surface. The reattachment line is visible all of the way to the trailing edge for small incidences, but only the initial part of it near the apex is easy to identify with increasing incidence. This feature is very similar to the near-surface patterns shown in Fig. 10. The reattachment line moves toward the centerline of the wing with increasing incidence. Figure 12 shows the spanwise location of the reattachment line normalized by the local semispan for wind- and water-tunnel experiments as a function of incidence. The data for the water-tunnel experiments show that for lower Reynolds numbers reattachment generally occurs farther inboard. However, the trends are in both cases the same, with increasing incidence moving the reattachment line toward the wing centerline until, at $\alpha \approx 22$–23 deg for both cases, reattachment occurs at the centerline near the stall condition.

In Fig. 11, the secondary separation line reveals a change in curvature at around 30% of the chord length from the apex for $\alpha \leq 15$ deg. This is most likely to be a consequence of vortex breakdown for this nonslender wing rather than the transition of the boundary layer as discussed by Ref. 4. After the vortex breakdown reaches the apex, the secondary separation line moves outboard initially, but a kink develops toward the trailing edge of the wing, resulting in relatively large regions of separated flow as shown for $\alpha \geq 20$ deg, as indicated by an arrow in the figure. The location of the kink moves upstream with increasing incidence, and stalled flow covers the wing surface very rapidly.

As the largest buffeting is observed around $\alpha = 20$ deg and there is no vortex breakdown at this incidence, it is suggested that the shear-layer reattachment is responsible for large buffeting. This is supported by examination of unsteady aspects as summarized next.

Fluctuating Flow

Magnitude of the rms velocity near the wing surface is shown in Fig. 13. Fewer streamlines have been included in this figure to aid clarity. Underneath the path of the vortex axis lies a region of high rms velocity for $\alpha = 15$ deg. This footprint of vortex axis kinks and widens at the point of breakdown. The maximum velocity fluctuations occur just underneath the vortex axis after the point of breakdown, in this case at $x/c \approx 0.45$, a feature that is also observed over slender wings.[12] Because the vortex breakdown has reached the apex of the wing by $\alpha = 20$ deg, the nature of the flow unsteadiness is different at this incidence. The largest velocity fluctuations are

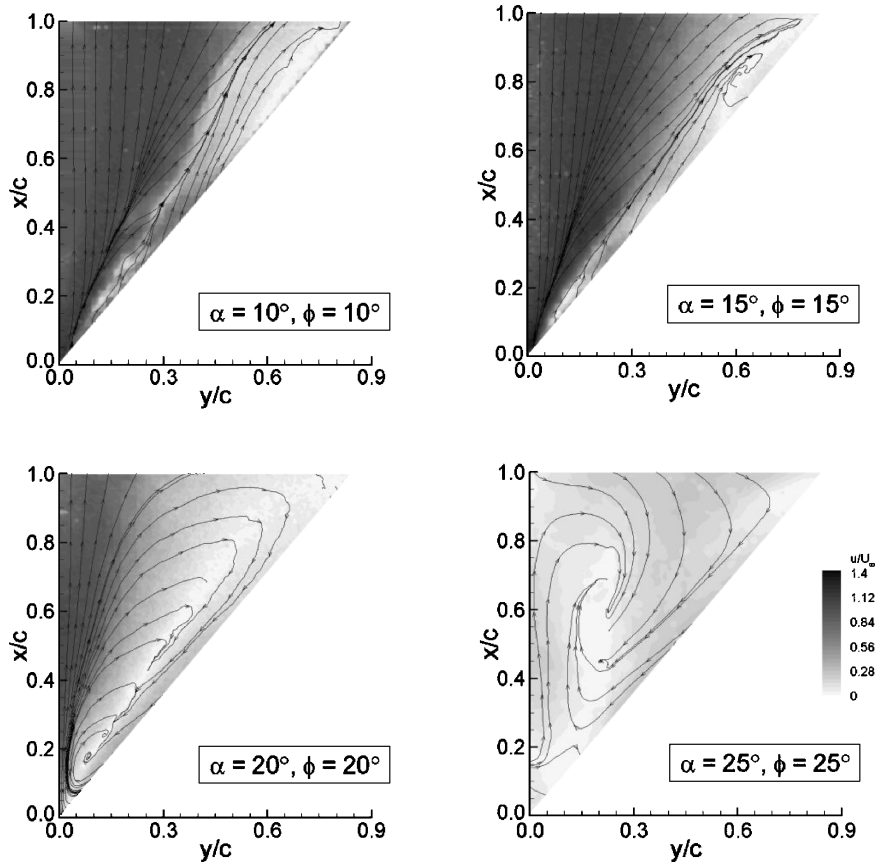

Fig. 10 Magnitude of time-averaged velocity and streamline pattern near the wing surface in water-tunnel experiments.

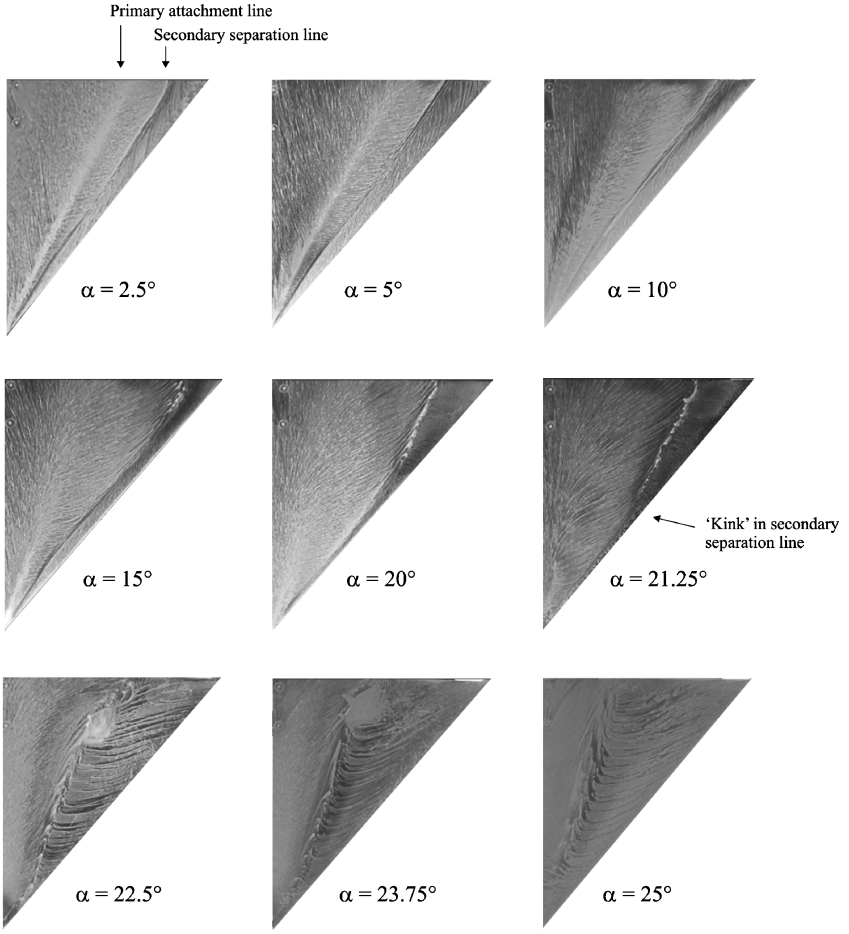

Fig. 11 Surface flow patterns at selected incidences in wind-tunnel experiments.

observed near the wing centerline in the region of the apex and just outboard along the reattachment line. This is in agreement with previous findings of Honkan and Andreopoulos,[24] who reported that the shear-layer reattachment zone is associated with high-turbulence activities. Again the buffeting of the flexible wing reaches a maximum around this angle of attack. Hence, unlike for slender delta wings, vortex breakdown phenomenon is not the most important source of buffeting. As the reattachment line occurs on the wing surface for nonslender wings with increasing incidence, the impingement of the shear layer onto the wing surface can generate large buffeting.

By $\alpha = 25$ deg, flow has become completely stalled with very low time-averaged velocity and very low rms velocity near the wing

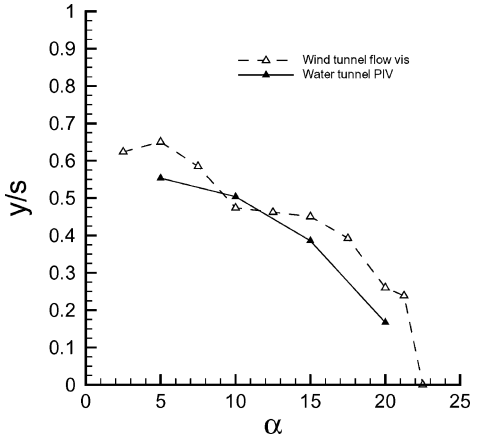

Fig. 12 Variation of spanwise location of reattachment line with incidence for water-tunnel and wind-tunnel models.

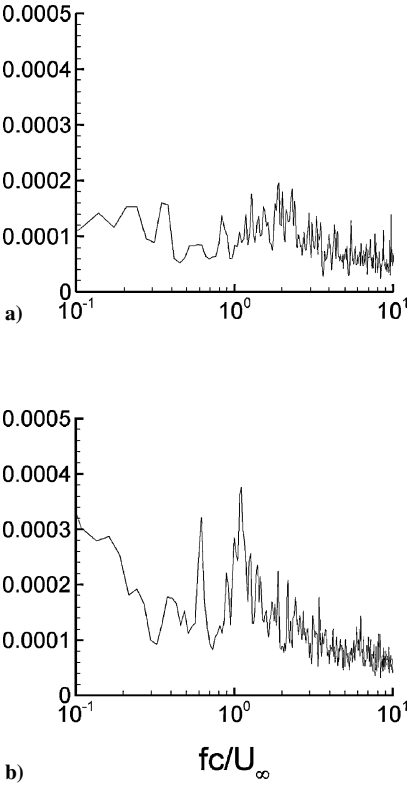

Fig. 14 Power spectrum of velocity fluctuations near the wing surface for a) $\alpha = 15$ deg ($x/c = 0.7$, $y/c = 0.36$) and b) $\alpha = 20$ deg ($x/c = 0.7$, $y/c = 0.21$).

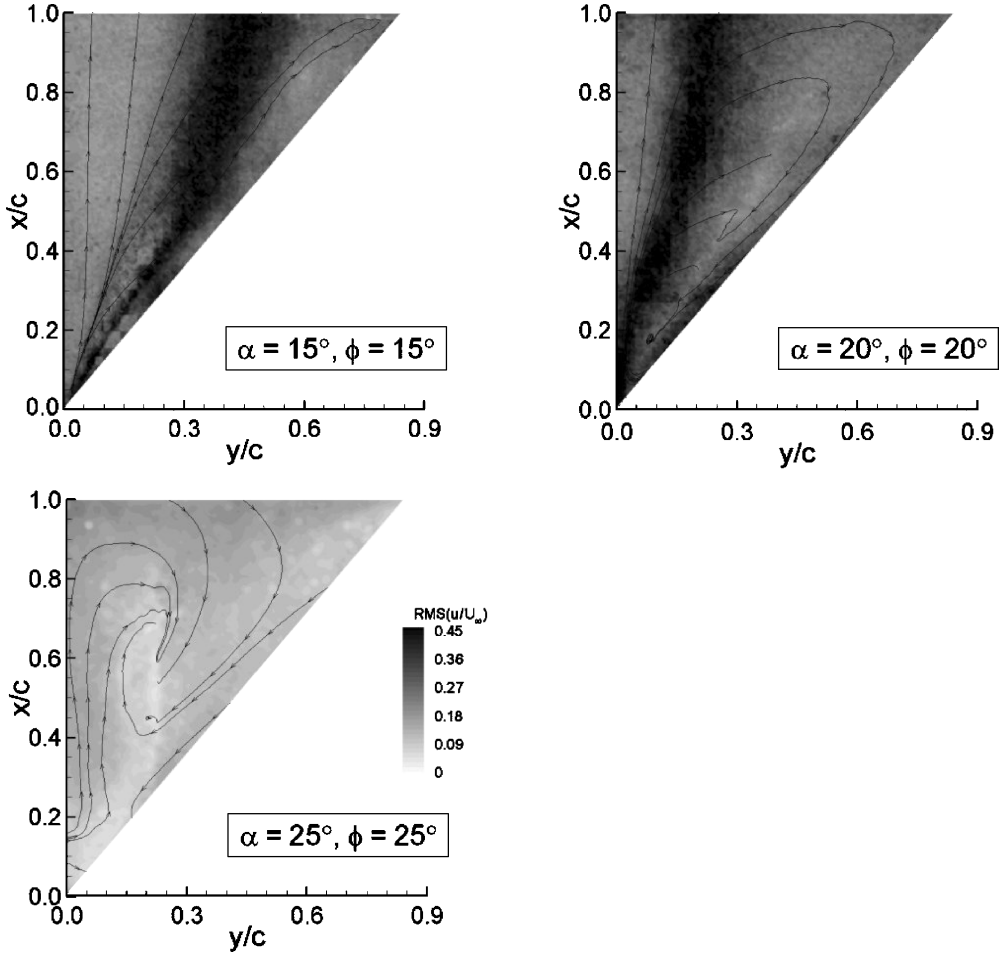

Fig. 13 Magnitude of rms velocity near the wing surface.

surface. Thus, once the stall angle has been passed and reattachment of the shear layer fails, minimal excitation of the wing structure occurs, as demonstrated by measurements of wing-tip acceleration for the flexible wing. This also coincides with the drop in lift associated with the stall.

Spectral characteristics of the velocity near the wing surface were studied with the LDV measurements in the breakdown wake for $\alpha = 15$ deg and in the reattachment region for $\alpha = 20$ deg. Some examples of the velocity spectra taken at a location with maximum fluctuations are shown in Fig. 14. The results for $\alpha = 15$ deg show that the velocity fluctuations exhibit broad frequency spectra, with a very broad peak centered around $fc/U_\infty \approx 2$, which is very different from the single dominant frequency observed for slender wings because of the helical mode instability. This observation is in agreement with the results of the direct numerical simulations[10] for a low sweep angle. In the $\alpha = 20$ deg case, there exist low-frequency oscillations in the reattachment zone. There are also two distinct peaks at $fc/U_\infty \approx 0.6$ and $fc/U_\infty \approx 1.2$, which are presumably related to the shear-layer instabilities and vortex pairing process. Similar "double-peak" spectra were observed for surface-pressure fluctuations in the reattachment region for $\Lambda = 40$ deg swept diamond wings.[25,26] Both references report dominant frequencies in the range of $fc/U_\infty = 1 - 2$, which are comparable to those reported in this paper for $\Lambda = 50$ deg. Although the shear-layer reattachment process is physically very different from the helical mode instability for slender wings, the measured frequencies in this paper and in Refs. 25 and 26 are in a similar range as slender wings.[12]

Conclusions

An experimental study was conducted to understand the unsteady vortex flows and buffeting response of a nonslender delta wing with 50-deg leading-edge sweep angle. Particle-image-velocimetry (PIV) and laser-Doppler-velocimetry (LDV) measurements, surface flow visualization, force balance measurements, and wing-tip acceleration measurements were used. It was found that there is a profound effect of Reynolds number on the structure of vortical flows. The breakdown of the leading-edge vortices is delayed significantly, and the vortices form more inboard at low Reynolds numbers. The secondary vortex effectively splits the primary vortex into two separate concentrations of vorticity, resulting in a dual vortex structure at small incidences. This dual vortex structure diminishes, and a single primary vortex is observed at higher incidences. At higher Reynolds numbers (on the order of 3×10^4) the flow approaches an asymptotic state, with further increases in the Reynolds number resulting in only small variations in the location of vortex core and breakdown.

Even at low angles of attack such as a few degrees, there are vortical flows and indication of vortex breakdown. But vortex breakdown is weak and difficult to identify, as there is no complete flow stagnation. The velocity fluctuations near the wing surface and the corresponding buffeting level are relatively small. With increasing angle of attack, the vortex breakdown becomes similar to but is not as abrupt as those observed over slender delta wings. The conical breakdown wake is naturally unsteady, and the maximum velocity fluctuations near the wing surface are observed just underneath the vortex axis. The corresponding buffeting level is relatively large. But the maximum buffeting occurs prior to the stall, after the vortex breakdown has reached the apex of the wing. The largest velocity fluctuations near the wing surface are observed along the reattachment line. Hence, the shear-layer reattachment, rather than the vortex breakdown phenomenon, is the most important source of increasing buffet in the prestall region as incidence is increased. The dominant frequencies are similar to those reported in experiments on low-sweep delta wings and also not much different from those of slender wings in spite of the differences in the flow. With further increase in incidence, the shear-layer reattachment becomes impossible, resulting in very low-velocity fluctuations near the wing surface and a precipitous fall in the rms wing tip acceleration.

Acknowledgments

This material is based on work supported by the European Office of Aerospace Research and Development, Air Force Office of Scientific Research, Air Force Research Laboratory, under Contract F61775-02-C4024. The authors acknowledge the assistance of A. McClain and S. Matthews in conducting wind-tunnel experiments.

References

[1]Rockwell, D., "Three-Dimensional Flow Structure on Delta Wings at High Angle-of-Attack: Experimental Concepts and Issues," AIAA Paper 93-0050, Jan. 1993.

[2]Visbal, M. R., "Computational and Physical Aspects of Vortex Breakdown on Delta Wings," AIAA Paper 95-0585, Jan. 1995.

[3]Delery, J. M., "Aspects of Vortex Breakdown," *Progress in Aerospace Sciences*, Vol. 30, No. 1, 1994, pp. 1–59.

[4]Earnshaw, P. B., and Lawford, J. A., "Low-Speed Wind-Tunnel Experiments on a Series of Sharp-Edged Delta Wings," Aeronautical Research Council, Repts. and Memoranda No. 3424, London, March 1964.

[5]Wentz, W. H., and Kohlman, D. L., "Vortex Breakdown on Slender Sharp-Edged Wings," *Journal of Aircraft*, Vol. 8, No. 3, 1971, pp. 156–161.

[6]Miau, J. J., Kuo, K. T., Liu, W. H., Hsieh, S. J., Chou, J. H., and Lin, C. K., "Flow Developments Above 50-Deg Sweep Delta Wings with Different Leading-Edge Profiles," *Journal of Aircraft*, Vol. 32, No. 4, 1995, pp. 787–794.

[7]Ol, M. V., and Gharib, M., "Leading-Edge Vortex Structure of Nonslender Delta Wings at Low Reynolds Number," *AIAA Journal*, Vol. 41, No. 1, 2003, pp. 16–26.

[8]Gursul, I., Taylor, G., and Wooding, C., "Vortex Flows over Fixed-Wing Micro Air Vehicles," AIAA Paper 2002-0698, Jan. 2002.

[9]Taylor, G. S., Schnorbus, T., and Gursul, I., "An Investigation of Vortex Flows over Low Sweep Delta Wings," AIAA Paper 2003-4021, June 2003.

[10]Gordnier, R. E., and Visbal, M. R., "Higher-Order Compact Difference Scheme Applied to the Simulation of a Low Sweep Delta Wing Flow," AIAA Paper 2003-0620, Jan. 2003.

[11]Menke, M., and Gursul, I., "Unsteady Nature of Leading Edge Vortices," *Physics of Fluids*, Vol. 9, No. 10, 1997, pp. 2960–2966.

[12]Gursul, I., "Unsteady Flow Phenomena over Delta Wings at High Angle-of-Attack," *AIAA Journal*, Vol. 32, No. 2, 1994, pp. 225–231.

[13]Gursul, I., and Xie, W., "Buffeting Flows over Delta Wings," *AIAA Journal*, Vol. 37, No. 1, 1999, pp. 58–65.

[14]Gordnier, R., and Visbal, M. R., "Unsteady Vortex Structure over a Delta Wing," *Journal of Aircraft*, Vol. 31, No. 1, 1994, pp. 243–248.

[15]Menke, M., Yang, H., and Gursul, I., "Experiments on the Unsteady Nature of Vortex Breakdown over Delta Wings," *Experiments in Fluids*, Vol. 27, No. 3, 1999, pp. 262–272.

[16]Redinoitis, O. K., Stapountzis, H., and Telionis, D. P., "Periodic Vortex Shedding over Delta Wings," *AIAA Journal*, Vol. 31, No. 9, 1993, pp. 1555–1561.

[17]Gray, J., Gursul, I., and Butler, R., "Aeroelastic Response of a Flexible Delta Wing Due to Unsteady Vortex Flows," AIAA Paper 2003-1106, Jan. 2003.

[18]Gordnier, R. E., and Visbal, M. R., "Computation of the Aeroelastic Response of a Flexible Delta Wing at High Angles of Attack," AIAA Paper 2003-1728, 2003.

[19]Hart, D. P., "The Elimination of Correlation Errors in PIV Processing," 9th International Symposium on Applications of Laser Techniques to Fluid Mechanics, Lisbon, July 1998.

[20]Lamar, J. E., Brandon, J., and Johnson, T. D., Jr., "Vortex Features of F-106B Aircraft at Subsonic Speeds," AIAA Paper 93-3471, 1993.

[21]Traub, L. W., Moeller, B., and Rediniotis, O., "Low-Reynolds-Number Effects on Delta-Wing Aerodynamics," *Journal of Aircraft*, Vol. 35, No. 4, 1998, pp. 653–656.

[22]Moore, D. W., and Pullin, D. I., "Inviscid Separated Flow over a Non-Slender Delta Wing," *Journal of Fluid Mechanics*, Vol. 305, 1995, pp. 307–345.

[23]Delery, J. M., "Robert Legendre and Henri Werle: Toward the Elucidation of Three-Dimensional Separation," *Annual Review of Fluid Mechanics*, Vol. 33, 2001, pp. 129–154.

[24]Honkan, A., and Andreopoulos, J., "Instantaneous Three-Dimensional Vorticity Measurements in Vortical Flow over a Delta Wing," *AIAA Journal*, Vol. 35, No. 10, 1997, pp. 1612–1620.

[25]Woods, M. I., "An Investigation of Buffet over Low-Observable Planforms," Ph.D. Dissertation, Dept. of Mechanical Engineering, Univ. of Bath, Bath, England, U.K., July 1999.

[26]Lynn, R. J., Gib, J., and Shires, A., "Buffet Tests on a 40 Degree Diamond Wing Planform—Model M2391," DERA, Rept. DERA/MSS4/TR980309/1.0, London, Aug. 1998.

K. Fujii
Associate Editor